Delft University of Technology

Document Version
Final published version

Licence
CC BY

Citation (APA)
Liu, H., Lodha, S., van der Zant, H. S. J., Steeneken, P. G., & Verbiest, G. J. (2026). Optomechanical method for characterizing thermal transport across suspended van der Waals interfaces. *2D Materials*, *13*(4), Article 045009. https://doi.org/10.1088/2053-1583/aeaa6b

Important note
To cite this publication, please use the final published version (if applicable).
Please check the document version above.

Copyright
In case the licence states “Dutch Copyright Act (Article 25fa)”, this publication was made available Green Open Access via the TU Delft Institutional Repository pursuant to Dutch Copyright Act (Article 25fa, the Taverne amendment). This provision does not affect copyright ownership.
Unless copyright is transferred by contract or statute, it remains with the copyright holder.

Sharing and reuse
Other than for strictly personal use, it is not permitted to download, forward or distribute the text or part of it, without the consent of the author(s) and/or copyright holder(s), unless the work is under an open content license such as Creative Commons.

Takedown policy
Please contact us and provide details if you believe this document breaches copyrights.
We will remove access to the work immediately and investigate your claim.

This work is downloaded from Delft University of Technology.

2D Materials

PURPOSE-LED PUBLISHING™

PAPER • **OPEN ACCESS**

Optomechanical method for characterizing thermal transport across suspended van der Waals interfaces

To cite this article: Hanqing Liu *et al* 2026 *2D Mater.* **13** 045009

View the article online for updates and enhancements.

You may also like

- Strongly tunable anisotropic thermal transport in MoS_2 by strain and lithium intercalation: first-principles calculations
Shunda Chen, Aditya Sood, Eric Pop et al.
- *(Invited, Digital Presentation)* Ultra-Low Thermal Conductance across Hetero-Structured Four-Layered Van Der Waals Materials
Kazuhiro Yanagi
- Interface thermal conductance of van der Waals monolayers on amorphous substrates
Gabriela C Correa, Cameron J Foss and Zlatan Aksamija

This content was downloaded from IP address 131.180.130.24 on 15/10/2026 at 08:14

2D Materials

Check for updates

PAPER

OPEN ACCESS

RECEIVED
30 March 2026

REVISED
9 September 2026

ACCEPTED FOR PUBLICATION
21 September 2026

PUBLISHED
1 October 2026

Original content from this work may be used under the terms of the Creative Commons Attribution 4.0 licence.

Any further distribution of this work must maintain attribution to the author(s) and the title of the work, journal citation and DOI.

Optomechanical method for characterizing thermal transport across suspended van der Waals interfaces

Hanqing Liu[1,2,*], **Saurabh Lodha**[3], **Herre S J van der Zant**[4], **Peter G Steeneken**[2,4] and **Gerard J Verbiest**[2,*]

[1] College of Electronic Science and Technology, National University of Defense Technology, Deya Road 109, 410073 Changsha, People's Republic of China
[2] Department of Precision and Microsystems Engineering, Delft University of Technology, Mekelweg 2, Delft, 2628 CD, The Netherlands
[3] Department of Electrical Engineering, Indian Institute of Technology Bombay, Mumbai, Powai 400076, India
[4] Kavli Institute of Nanoscience, Delft University of Technology, Lorentzweg 1, Delft, 2628 CJ, The Netherlands
[*] Authors to whom any correspondence should be addressed.

E-mail: liuhanqing@nudt.edu.cn and G.J.Verbiest@tudelft.nl

Keywords: suspended vdW interfaces, thermal boundary conductance, optomechanical measurement

Supplementary material for this article is available online

Abstract

For the development of nanoscale electronics and photonics using atomically thin two-dimensional (2D) materials, it is important to realize van der Waals (vdW) interfaces with low thermal resistance, to minimize performance reduction caused by heat accumulation. However, characterizing the thermal interface resistance between vdW materials is still a challenge. Here, we introduce a novel optomechanical methodology to characterize the thermal transport across interfaces in suspended 2D heterostructures. We first determine the specific heat and thermal conductivity as a function of temperature for the upper and lower multilayer 2D materials separately and then extract the thermal boundary conductance (TBC) of the heterostructure from its thermal time constant. We obtain a TBC of 3.23 ± 1.43 and 4.32 ± 2.56 MWm^2K^{-1} for the suspended $FePS_3/WSe_2$ and $MoS_2/FePS_3$ interfaces, respectively, which are comparable to values reported in the literature. Moreover, they agree with a Debye model including the acoustic impedance mismatch of acoustic phonons. This work enables efficient thermal management down to the nanoscale and offers new insights into energy dissipation in vdW heterostructures.

1. Introduction

The material class of two-dimensional (2D) materials comprises a wide range of mechanically flexible and atomically thin compounds for the next-generation electronic, photonic, magnetoelectric and thermoelectric applications [1–4]. For creating unique designer materials or devices that address these applications, stacking 2D materials is needed to tailor the desired functionality [5, 6]. However, to ensure heat can be transported away efficiently, low thermal resistance at the interfaces between the 2D materials is important to prevent temperature rise and concomitant performance degradation [7]. The heat generated in stacked van der Waals (vdW) devices, i.e. 2D heterostructures, travels both in-plane through each 2D material layer, the substrate, and out-of-plane direction across vdW interfaces including 2D/2D and 2D/substrate interfaces. These heat transport pathways are mainly characterized by the thermal conductivity of the materials and the thermal boundary conductance (TBC) on the interfaces, respectively [8, 9]. As a result of the weak vdW bonding between vdW interfaces, large thermal isolation can arise which dominates the heat flow in the system [10]. Therefore, characterizing the thermal transport across vdW interfaces is critical for optimizing the thermal management and thereby enable a pathway towards high performance 2D heterostructures.

So far, a variety of experimental techniques have been developed to determine the TBC at vdW interfaces, with transient electrical [11–13] and steady-state Raman thermometry [14–16] emerging as the most widely adopted approaches. However, both methods pose significant challenges: electrical thermometry requires complicated device fabrication and is affected by thermal contact resistance effects, while Raman thermometry typically suffers from

© 2026 The Author(s). Published by IOP Publishing Ltd

limited temperature resolution, resulting in substantial measurement uncertainties. These methodological constraints have compromised the precision of thermal transport characterization across vdW interfaces, contributing to the considerable variation in the reported TBC values among existing studies. For example, the TBC values for the graphene/SiO_2 interface measured by electrical thermometry vary from 83 to 178 MW m^{-2}/K at room temperature [17], and are much higher than the values below 35 MW m^{-2}/K typically obtained by Raman thermometry [8, 18].

In this Letter, we demonstrate an optomechanical non-contact method for characterizing thermal transport across suspended vdW interfaces. The proposed methodology allows us to simultaneously extract the thermal expansion coefficient, the specific heat and the in-plane thermal conductivity of different type of multilayer 2D materials, and finally determine the TBC across suspended vdW interface. It involves determining the cool down time of a suspended membrane that is heated by a power-modulated laser and measuring its deflection, that is driven by thermal expansion with a second laser [19, 20]. Accordingly, both the temperature-dependent mechanical resonance frequency and thermal time constant of the membrane are measured. A major advantage of the method is that no physical contact needs to be made to the suspended 2D heterostructure, such that its pristine properties are probed and no complex device fabrication is needed. Here we focus on the thermal transport of vdW interface between transition-metal phosphorus trisulfides and dichalcogenides, which has never been investigated before. Our results on the TBC of $FePS_3$/WSe_2 and MoS_2/$FePS_3$ show good agreement with reported values in the literature.

2. Fabrication and methodology

We fabricate 2D nanomechanical resonators by transferring two flakes of different 2D materials on the same chip, such that the flakes partly overlap. Since the chip contains circular cavities in a SiO_2 layer on Si, with a depth of 285 nm and radius of 3 μm, suspended membranes including both of the individual multilayer 2D materials and the stacked heterostructure are formed. As illustrated in figure 1(a), devices D1 and D2 are made of suspended $FePS_3$ and WSe_2 membranes, respectively, while the central overlapping region forms a $FePS_3$(upper)/WSe_2(lower) heterostructure, device D3. To determine the Young's modulus E of each membrane, we use the AFM to indent the center of the suspended area with a force while measuring the cantilever indentation [21]. As listed in table 1, we extract $E = 98.3$ GPa and 93.1 GPa for devices D1 and D2, respectively, which are in good agreement with typical values found in literature [22, 23]. In addition, we fabricate another heterostructure resonator device made of MoS_2(upper)/$FePS_3$(lower) flakes, and further experimentally test it with the same methodology. All details about the thickness and Young's modulus measurement of devices D1–D3, as well as the MoS_2/$FePS_3$ device can be found in SI section 1.

The setup for the optomechanical measurements [24, 25], is shown in figure 1(b). A power-modulated blue diode laser ($\lambda = 405$ nm) photothermally actuates the resonator, while a He–Ne laser ($\lambda = 632$ nm), of which the reflected laser power depends on the position of the membrane, is used to detect the motion of the resonator. The power-modulation of the blue laser is supplied by a vector network analyzer (VNA), which also analyzes the photodiode signal containing the reflected laser power and converts that to the response amplitude, $|z_f|$, of the resonator in the frequency domain (see figure 1(c)). All measurements were done in vacuum at a pressure below 10^{-5} mbar. In figure 1(d), $|z_f|$ shows a clear fundamental resonance peak in MHz frequencies, which can be fitted by a harmonic oscillator model given by $|z_f| = \frac{A_{\mathrm{res}} f_0^2}{Q\sqrt{(f_0^2 - f^2)^2 + (f_0 f/Q)^2}}$, where f_0 is the fundamental resonance frequency, f is the driving frequency, A_{res} is the vibration amplitude at resonance and Q is the quality factor. For device D1, we obtain a $f_0 = 9.53$ MHz and $Q = 160$. Moreover, we also find a maximum in the imaginary part of z_f at kHz frequencies (see figure 1(e)), which is attributed to the thermal expansion of the membrane that is time-delayed with respect to the modulated blue laser power, because it takes a time τ for the temperature of the membrane to rise [26]. The signal at driving frequencies f far below the resonance frequency f_0 can be expressed as:

$$z_f = \frac{A_{\mathrm{th}}}{i2\pi f\tau + 1}, \tag{1}$$

where A_{th} and τ are the thermal expansion amplitude and thermal time constant of the membrane, respectively. The red and blue laser powers are fixed at 0.9 and 0.13 MW respectively, which are low enough to ensure linear vibration of the resonators. We extract τ by fitting the measured imaginary part of z_f to equation (1) (see figure 1(e)). Here, we obtain the maximum of $\mathrm{Im}(z_f)$ at around 366.19 kHz for device D1, corresponding to $\tau = (2\pi \times 366.19\ \mathrm{kHz})^{-1} = 434.62$ ns.

3. Results

Figure 2(a) shows the equivalent model that describes the heat transport in the heterostructure resonator. To determine the TBC G, the thermal properties of pure $FePS_3$ and WSe_2 membranes, including the specific heat c_p and thermal conductivity k, need to

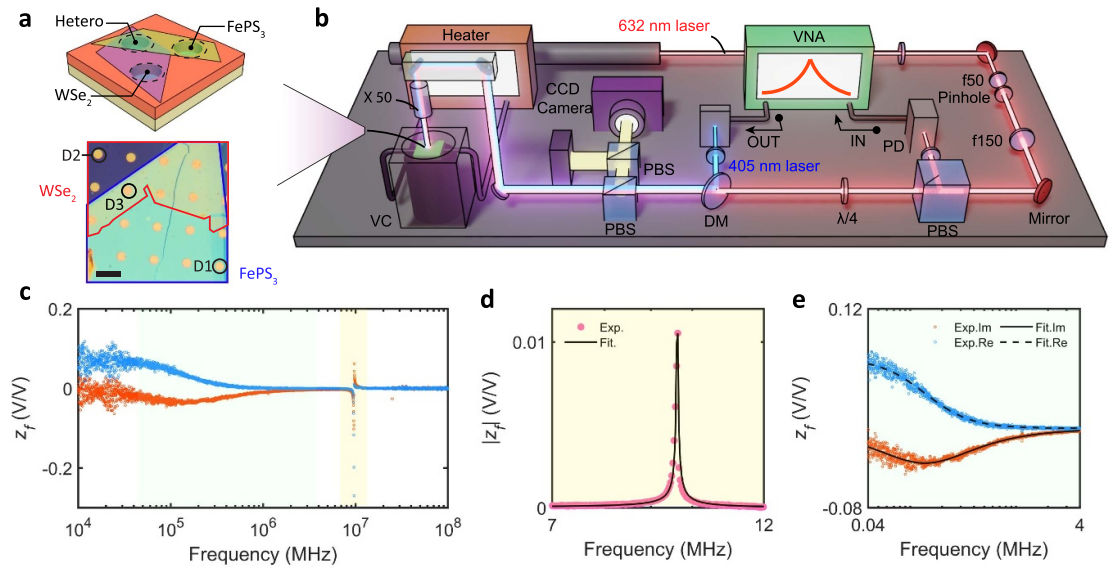


Figure 1. Sample characterization and experimental setup. (a) Schematic (top) and optical image (bottom) of the fabricated 2D resonators. Scale bar: 10 μm. D1, $FePS_3$ device; D2, WSe_2 device; D3, $FePS_3/WSe_2$ heterostructure device. (b) Setup of optomechanical measurement. VNA, vector network analyzer; PD, photodiode; PBS, polarized beam splitter; DM, dichroic mirror; VC, vacuum chamber. (c) Frequency response of device D1, including real (red) and imaginary (blue) parts of the motion z_f. (d) Resonant peak of device D1 measured at MHz regime (points), which is fitted with a harmonic model (drawn line) to extract the resonance frequency f_0 of device D1. (e) Thermal signal measured at kHz regime, including imaginary (red) and real (blue) parts. The imaginary part is fitted with equation (1) (drawn lines) to obtain the thermal time constant τ of device D1.

Table 1. Characteristics of devices D1 and D2, including radius R, thickness t, mass density ρ, Young's modulus E, atomic mass M, Poisson ratio ν, Grüneisen parameter γ. The values of ρ, M, ν and γ are taken from literature [22, 23, 27].

	R (μm)	t (nm)	ρ (kg m^{-3})	E (GPa)	M (g mol^{-1})	ν	γ
D1 ($FePS_3$)	3	34.5	3375	93.1	183	0.304	1.80
D2 (WSe_2)	3	8.6	9320	98.3	342	0.19	0.79

be determined in advance. We start by heating up the fabricated devices D1 and D2. When changing the temperature, the thermal expansion coefficient (TEC) α_m of the membrane, which is higher than that of the silicon substrate α_{Si}, changes the strain in the membrane. This results in a resonance frequency change of 2D nanomechanical resonators, which can be used for probing the thermal properties [28, 29]. As shown in figure 2(c), we observe a decrease of f_0 with increasing T for device D2, which is in agreement with trends shown in literature [30] and can be attributed to a reduction in tension when the material thermally expands. Following our previous study [19], the relation between f_0 and the thermally induced in-plane displacement U for a clamped circular plate is given by:

$$\frac{df_0^2}{dT} = c_t \frac{dU}{dT}, \tag{2}$$

where $\frac{dU}{dT} = -R[\alpha_m(T) - \alpha_{Si}(T)]$, ν is the Poisson ratio, $d = 2R$ is the diameter of the membrane, and $c_t = \frac{13.34E}{\pi^2 d^2 \rho(1-\nu)}$. The flow chart (left) depicted in figure 2(b) exhibits how optomechanical measurements enable a precise pathway for studying the thermal properties of heterostructure resonator. Firstly, we extract the TEC $\alpha_m(T)$ of the membrane from the obtained $\frac{dU}{dT}$ using equation (2), where the values of $\alpha_{Si}(T)$ are taken from literature [31]. Next, the specific heat c_p of the membrane is extracted directly from α_m using the thermodynamic relation $c_p = 3\alpha_m K/\gamma\rho$ [23], where $K = \frac{E}{3(1-2\nu)}$ is the bulk modulus, and γ is the Grüneisen parameter of the membrane taken from literature (see table 1). As shown in figure 3(a), the obtained $c_{p2}(T)$ for device D2 is about 100±2 Jkg^{-1}K^{-1}, which is comparable to the literature values [22]. Then, by solving the heat equation in the membrane with an appropriate initial temperature distribution and well-defined boundary conditions, the thermal conductivity of the membrane can be extracted from the measured τ and the obtained c_p through:

$$\tau_j = \frac{R^2 c_{pj}\rho_j}{\mu_j^2 k_j}, j = 1, 2 \tag{3}$$

where k_j is the in-plane thermal conductivity of 2D materials and the in-plane diffusive eigenvalue for single-layer circular plate is $\mu_j^2 = 5$ [19]. Hence, by substituting the obtained c_{p2} and the measured τ_2 (figure 2(e)) into equation (3), we extract $k_2 = 7.6 \pm 1.2$ Wm^{-1}K^{-1} for device D2 (see figure 3(b)). In

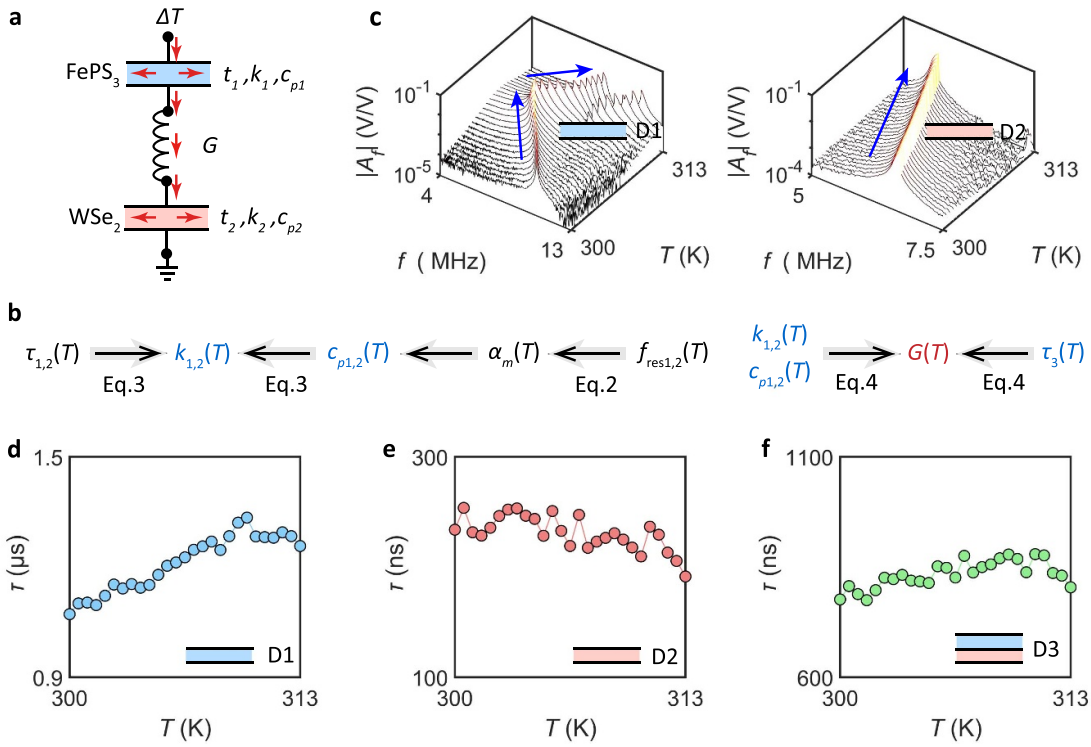


Figure 2. Temperature-dependent optomechanical measurements on devices D1-D3. (a) Equivalent model of heat propagation on $FePS_3/WSe_2$ membrane. (b) The proposed procedure to determine the values of TBC G. (c) Resonant peak measured as a function of temperature T for devices D1 and D2. **d-f** Thermal time constant τ measured as a function of T for devices D1-D3, respectively.

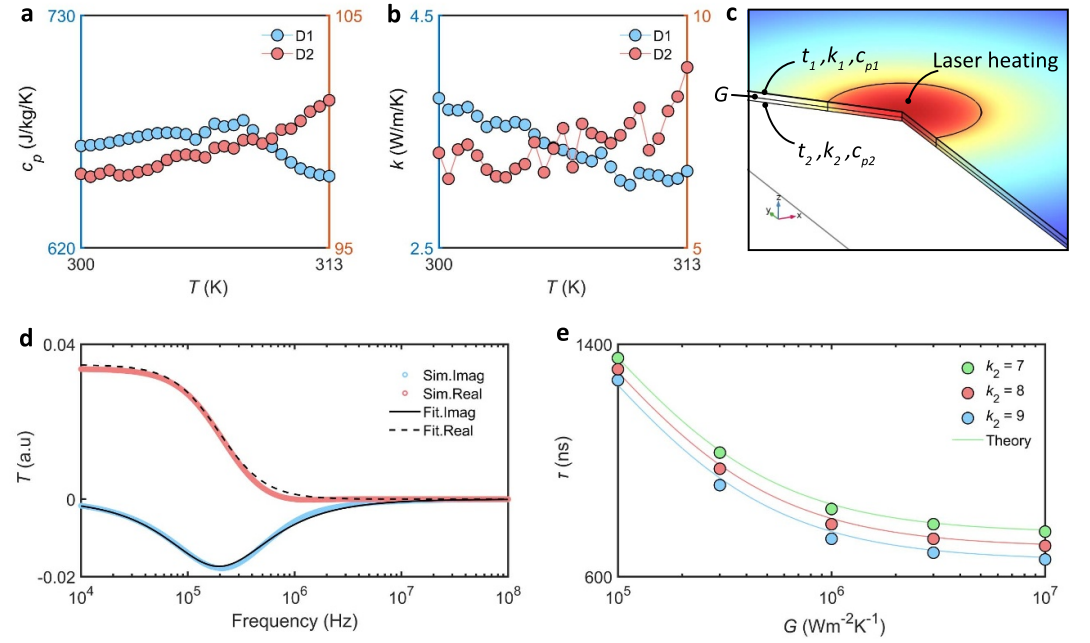


Figure 3. Characterizing the thermal properties of 2D resonators. (a) Specific heat c_p and (b) in-plane thermal conductivity k as a function of temperature T for devices D1 and D2, respectively. (c) Schematic diagram of 2D heterostructure resonator in COMSOL simulation software. (d) Temperature distribution of the membrane versus heating rate. Points, simulation results; drawn lines, fitting by equation (1). (e) Estimations of thermal time constant τ_3 versus G for device D3. Points, simulation results; drawn lines, calculation by equation (4).

the following we will explain how to extract the TBC from the measured thermal time constant of the heterostructure.

For device D1, we observe an initial decrease in f_0 with increasing T towards a minimum frequency, followed by a continuous increase. This is attributed to the thermally-induced buckling of mechanical resonators, caused by a loaded compression since $\alpha_m > \alpha_{Si}$. In this case, a factor δ connected with the deflection of the membrane is added to equation (2) in order to accurately determine the relation between f_0 and U under buckling [25]. The detailed expression of δ can be found in SI section 1. We further extract $c_{p1} = 665 \pm 11$ Jkg^{-1}K^{-1} and $k_1 = 3.4 \pm 0.3$ Wm^{-1}K^{-1} for device D1, as plotted in figures 3(a) and (b), respectively, which are comparable to the literature values [27].

After characterizing the thermal properties of $FePS_3$ and WSe_2 membrane separately, we move on to the estimation of TBC G in heterostructure device D3. To figure out the dependence of τ_3 on G, we employed a 3D heat transport model in COMSOL, as illustrated in figure 3(c). The structural parameters R, $h_{1,2}$, $\rho_{1,2}$ are used as given for $FePS_3$ and WSe_2 membranes. The laser pulse with harmonic perturbation irradiates at the center of the top surface, and the spot size is fixed as its realistic value $R_0 = 0.5$ μm. The boundary conditions on the interface are set as $k_{1z}\frac{\partial T_1}{\partial z} = k_{2z}\frac{\partial T_2}{\partial z} = -G(T_1 - T_2)$, where T_1 and T_2 are the temperature distribution of $FePS_3$ and WSe_2 membrane, respectively, k_{1z} and k_{2z} are their corresponding out-of-plane thermal conductivity. Using $c_{p1} = 690$ J kg^{-2}, $c_{p2} = 90$ J kg^{-2}, $k_1 = k_{1z} = 3.5$ W m^{-1} K^{-1}, $k_2 = k_{2z} = 8$ W m^{-1} K^{-1} and $G = 10$ MW m^{-2}/K in the model, we simulate the normalized temperature distribution of the heterostructure as plotted in figure 3(d). A thermal time constant τ_3 of 779.5 ns can be extracted by fitting the imaginary part of T with equation (1). We then obtain a negative dependence of τ_3 on G by the simulation, as shown in figure 3(e) (solid points), indicating that a higher TBC on the vdW interface will accelerate the overall heat transfer of the system. To shed light on the physical mechanism of τ_3 versus G, we solve the Fourier heat conduction equations in cylindrical coordinates for a bi-layered circular plate with similar boundary conditions as in the COMSOL simulation (see SI section 2 for derivation), which allows to obtain the expression:

$$\tau_3 = \tau_{3,int} + \frac{c_{p1}\rho_1}{k_1\eta^2 + \frac{G}{t_1}}, \tag{4}$$

where the in-plane eigenvalue is $\eta^2 = \left(\frac{2.4048}{R}\right)^2$. The first part in equation (4) represents the intrinsic thermal time constant of the heterostructure device when $G \to +\infty$. Considering the case of two-layer 2D materials connected in parallel, we have $\tau_{3,int} = \frac{R^2(c_{p1}t_1\rho_1 + c_{p2}t_2\rho_2)}{\mu_3^2(t_1k_1 + t_2k_2)}$, where the in-plane diffusive eigenvalue μ_3^2 for heterostructure is determined as 5.36 by COMSOL simulation (see SI section 3). The second part in equation (4) represents the contribution from G-dominated thermal diffusivity, which is obtained from the solution of Fourier heat conduction equations. Note that the contributions from k_{1z} and k_{2z} on τ_3 are negligible for the fabricated devices, the anisotropy between in-plane and out-of-plane thermal conductivity for 2D vdW materials does not play a role in our proposed methodology (see SI section 2). As shown in figure 3(e), we obtain a good agreement of τ_3 versus G between the estimation and simulation under different k_2. As a result, through substituting the extracted $c_{p1,2}$, $k_{1,2}$ and the measured τ_3 (see figure 2(f)) into equation (4), we finally extract G about 3.23 ± 1.43 MWm^{-2}K^{-1} for device D3 in the range from 300 to 313 K, as shown in figure 4(a). Using the same approach, we also determine $G = 4.32 \pm 2.56$ MWm^{2}K^{-1} for the fabricated $MoS_2/FePS_3$ heterostructure resonator (see SI section 1 for details).

The obtained G for our fabricated devices are comparable to the reported values for vdW interfaces made of MoS_2, WSe_2 or graphene [8, 32, 33], as shown in figure 4(b) (points). To better understand the physical mechanism of TBC, we follow the literature [8, 34] and use a Debye model wherein G is proportional to the product of the overlapping phonon density of states (PDOS) areas of the two materials, the mass density mismatch, and the derivative of the Bose–Einstein distribution function with respect to temperature (see SI section 4 for details). Here, we consider the PDOS for both in-plane (LA and TA) phonons and flexural (ZA) phonons, which are known to dominate the heat conduction in 2D heterostructure devices [20, 35]. As plotted in figure 4(b) (drawn line), the theoretical estimation of G by the Debye model matches well with our experimental results as well as the other reported values from literature. We conclude that the characteristics of phonons in $FePS_3$ attribute to a small area of PDOS overlap at $FePS_3$-based vdW interface, resulting in the low values of TBC for our $FePS_3/WSe_2$ and $MoS_2/FePS_3$ devices in this work.

4. Discussion and conclusions

Compared to other methods for measuring the TBC of vdW interfaces, our proposed approach offers several advantages, as outlined in table 2. For instance, Raman thermometry requires large temperature changes to detect the frequency shifts in Raman mode, necessitating measurements over a broad temperature range to precisely determine the slope χ_T of the peak shift versus temperature. In the case of MoS_2, for example, χ_T is only cm^{-1}K^{-1}, which means given

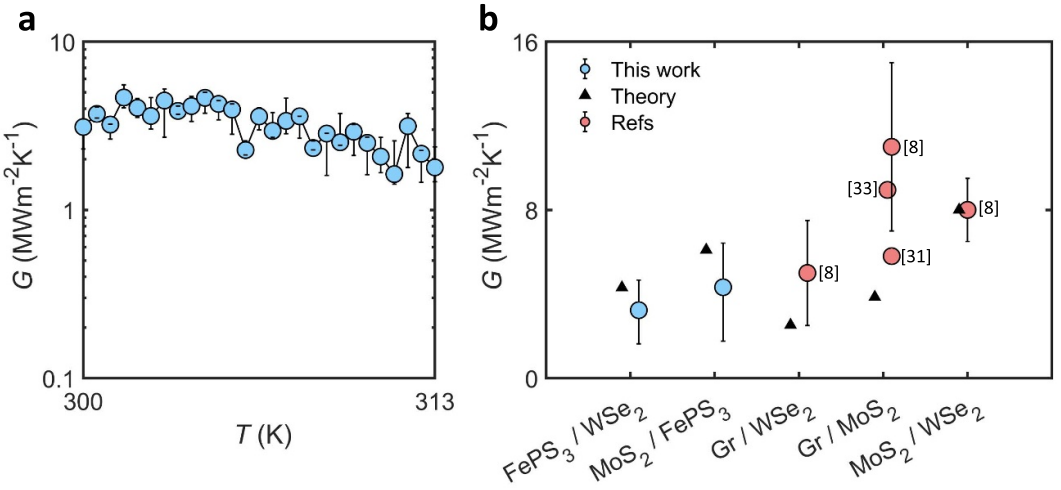


Figure 4. Quantifying TBC G in 2D heterostructure resonators. (a) Dependence of G on temperature T for device D3 from 300 to 313 K. (b) Comparison of the extracted G in this work with the reported values from literature. Black triangles, Theoretical estimation of G by the built Debye model.

Table 2. Comparison of different methods for measuring the TBC of vdW interfaces.

	Raman thermometry	Electrical thermometry	Optomechanics
Required temperature range	50−100 K [40, 41]	10−50 K [11]	$<$ 10 K
Sample preparation	Easy	Difficult	Easy
Applicability to 2D materials	Applicable	Limited	Applicable

a typical resolution limit of 0.25 cm^{-1} for a Raman microscope, a temperature rise of at least 20 K is needed to achieve reliable results [36]. In addition, the crosstalk of Raman modes in different 2D materials, e.g. MoS_2 and WS_2, will significantly affect the resolution of χ_T. For electrical-thermometry, either thick crystals or stiff 2D materials like graphene have to survive the complicated fabrication procedures including lithography and etching [37]. In contrast, for the presented contactless optomechanical method, one only needs to suspend membranes over cavities in a SiO_2/Si substrate, while the accuracy can be maintained within 0.1 K by using a sensitive heater. Moreover, we have verified the laser power dependence has no significant effect on the measured value of τ, so that the calibration of laser power as commonly adopted in Raman measurement is not necessary here [20]. Hence, our proposed methodology provides a precise and applicable platform for characterizing the thermal transport in vdW interfaces.

Considering a detection range of thermal signal from 10–1 MHz on VNA, our proposed methodology is applicable to 2D resonators that can be excited photothermally with thermal time constants τ between 160 ns and 16 μs. The 2D resonator should not be perfectly flat. In reality, inhomogeneities due to uneven adhesion or residues on the vdW interface could lead to multiple smaller corrugations and wrinkles superimposed in the membrane during thermal expansion, which could result in estimation errors when extracting specific heat from equation (2). Exfoliated 2D flakes are transferred onto the substrate using a dry transfer method, causing polymer residues and trapped bubbles on the vdW interfaces that could affect the measured TBC. As a result, we primarily selected the samples with clean surfaces for optomechanical measurement under optical microscope (see figure 1(a)). In addition, equations (3) and (4) are not applicable for monolayer and bilayer graphene, in which the scattering of acoustic phonons at the boundary between the supported and suspended parts of the 2D material dominates the value of the thermal time constant in measurement [20, 38].

It should be noted that μ_3^2 in equation (4) is related to the thickness and thermal properties of 2D materials, as well as the laser spot size. We verify that within the measured temperature range, the offset of μ_3^2 is below 0.2% compared to the fixed constant 5.36 (see SI section 3). In addition, given the same geometric and thermal characteristics of each layers, the opposite stacking order of heterostructure still results in different thermal time constants (see SI section 3). Moreover, our proposed methodology is more efficient when $G < 10$ MWm^2K^{-1}, where the slope of τ versus G is large enough to ensure a high accuracy of obtaining G by the measured τ (figure 3(e)). Finally, although the measured results of TBC in this work are well captured

by Debye model as shown in figure 4(b), we note that the acoustic phonon behaviors in 2D materials are highly related to their dispersion relation, surface tension, crystal grain size, and temperature [39]. These factors significantly affect the thermal transport in 2D heterostructure and should be further studied using the presented optomechanical methodology, which would help us to better understand the phonon scattering mechanisms in vdW interfaces and why the theoretical estimation of G by the Debye model can explain the experimental observations surprisingly well.

In conclusion, we demonstrated an optomechanical approach for probing the thermal transport across vdW interfaces in heterostructure resonators made of multilayer $FePS_3/WSe_2$ and $MoS_2/FePS_3$. By measuring the resonance frequency and thermal time constant of the fabricated devices as a function of temperature, we separately extract the specific heat and in-plane thermal conductivity of the upper and lower layers, and finally extract the TBC G on the vdW interface. The obtained values of G are in good agreement with values reported in the literature. Compared to other methods, the presented contactless optomechanical approach requires a smaller temperature range, allows for easy sample fabrication, and is applicable to any 2D materials. This work not only advances the fundamental understanding of phonon mismatch in vdW interfaces, but potentially also enables studies into the use of strain engineering and heterostructures for optimizing the heat flow in 2D nanodevices.

Acknowledgment

P G S and G J V acknowledge support by the Dutch 4TU federation for the Plantenna project. H S J v d Z and P G S acknowledge funding from the European Union's Horizon 2020 research and innovation program under Grant Agreement No. 881603. H L acknowledges the financial support from China Scholarship Council and the National Natural Science Foundation of China under Grant No. 62401592 and the Young Scientists Innovation Fund Project of National University of Defense Technology under Grant No. ZK24-10.

Data availability statement

All data that support the findings of this study are included within the article (and any supplementary files).

ORCID iDs

Hanqing Liu 0009-0004-5439-4057
Peter G Steeneken 0000-0002-5764-1218
Gerard J Verbiest 0000-0002-1712-1234

References

[1] Ban S, Nie X, Lei Z, Yi J, Vinu A, Bao Y and Liu Y 2023 Emerging low-dimensional materials for nanoelectromechanical systems resonators *Mater. Res. Lett.* **11** 21–52
[2] Steeneken P G, Dolleman R J, Davidovikj D, Alijani F and Van der Zant H S 2021 Dynamics of 2D material membranes *2D Mater.* **8** 042001
[3] Balandin A A 2011 Thermal properties of graphene and nanostructured carbon materials *Nat. Mater.* **10** 569–81
[4] Zhang K-X, Park G, Lee Y, Kim B H and Park J-G 2025 Magnetoelectric effect in van der Waals magnets *npj Quantum Mater.* **10** 6
[5] Zhang X, Zhang Y, Yu H, Zhao H, Cao Z, Zhang Z and Zhang Y 2023 Van der Waals-interface-dominated all-2D electronics *Adv. Mater.* **35** 2207966
[6] Park J-G, Zhang K-X, Cheong H, Kim J H, Belvin C A, Hsieh D, Ning H and Gedik N 2026 2D van der Waals magnets: from fundamental physics to applications *Rev. Mod. Phys.* **98** 025003
[7] Ong Z-Y and Bae M-H 2019 Energy dissipation in van der Waals 2D devices *2D Mater.* **6** 032005
[8] Vaziri S *et al* 2019 Ultrahigh thermal isolation across heterogeneously layered two-dimensional materials *Sci. Adv.* **5** eaax1325
[9] Huang J *et al* 2025 Enhancement of thermal boundary conductance between MoS2 and dielectric layer by self-assembled monolayers *Adv. Electron. Mater.* **11** 2400244
[10] Kim S E *et al* 2021 Extremely anisotropic van der Waals thermal conductors *Nature* **597** 660–5
[11] Li X, Yan Y, Dong L, Guo J, Aiyiti A, Xu X and Li B 2017 Thermal conduction across a boron nitride and SiO_2 interface *J. Phys. D: Appl. Phys.* **50** 104002
[12] Koh Y K, Bae M-H, Cahill D G and Pop E 2010 Heat conduction across monolayer and few-layer graphenes *Nano Lett.* **10** 4363–8
[13] Buckley D *et al* 2021 Anomalous low thermal conductivity of atomically thin InSe probed by scanning thermal microscopy *Adv. Funct. Mater.* **31** 2008967
[14] Yalon E *et al* 2017 Temperature-dependent thermal boundary conductance of monolayer MoS2 by Raman thermometry *ACS Appl. Mater. Interfaces* **9** 43013–20
[15] Liu X *et al* 2022 Energy Dissipation and Electrical Breakdown in Multilayer PtSe2 Electronics *ACS Appl. Mater. Interfaces* **14** 51122–9
[16] Yalon E *et al* 2017 Energy dissipation in monolayer MoS2 electronics *Nano Lett.* **17** 3429–33
[17] Chen Z, Jang W, Bao W, Lau C and Dames C 2009 Thermal contact resistance between graphene and silicon dioxide *Appl. Phys. Lett.* **95** 161910
[18] Yang J, Ziade E, Maragliano C, Crowder R, Wang X, Stefancich M, Chiesa M, Swan A K and Schmidt A J 2014 Thermal conductance imaging of graphene contacts *J. Appl. Phys.* **116** 023515
[19] Liu H, Brahmi H, Boix-Constant C, van der Zant H S, Steeneken P G and Verbiest G J 2024 Optomechanical methodology for characterizing the thermal properties of 2D materials *APL Mater.* **12** 021126
[20] Liu H, Lee M, Šiškins M, van der Zant H, Steeneken P and Verbiest G 2023 Tuning heat transport in graphene by tension *Phys. Rev. B* **108** L081401

[21] Castellanos-Gomez A, Poot M, Steele G A, Van Der Zant H S, Agraït N and Rubio-Bollinger G 2012 Elastic properties of freely suspended MoS2 nanosheets *Adv. Mater.* **24** 772–5
[22] Kumar S and Schwingenschlogl U 2015 Thermoelectric response of bulk and monolayer MoSe2 and WSe2 *Chem. Mater.* **27** 1278–84
[23] Siskins M, Lee M, Mañas-Valero S, Coronado E, Blanter Y M, van der Zant H S and Steeneken P G 2020 Magnetic and electronic phase transitions probed by nanomechanical resonators *Nat. Commun.* **11** 1–7
[24] Siskins M, Sokolovskaya E, Lee M, Mañas-Valero S, Davidovikj D, Van Der Zant H S and Steeneken P G 2021 Tunable strong coupling of mechanical resonance between spatially separated FePS3 nanodrums *Nano Lett.* **22** 36–42
[25] Liu H, Baglioni G, Boix-Constant C, van der Zant H S, Steeneken P G and Verbiest G J 2024 Enhanced sensitivity and tunability of thermomechanical resonance near the buckling bifurcation *2D Mater.* **11** 025028
[26] Dolleman R J, Lloyd D, Lee M, Bunch J S, Van Der Zant H S and Steeneken P G 2018 Transient thermal characterization of suspended monolayer MoS 2 *Phys. Rev. Mater.* **2** 114008
[27] Kargar F *et al* 2020 Phonon and thermal properties of quasi-two-dimensional FePS3 and MnPS3 antiferromagnetic semiconductors *ACS Nano* **14** 2424–35
[28] Ye F, Lee J and Feng P X-L 2018 Electrothermally tunable graphene resonators operating at very high temperature up to 1200 K *Nano Lett.* **18** 1678–85
[29] Zhang Z *et al* 2020 Coupling of magneto-strictive FeGa film with single-crystal diamond MEMS resonator for high-reliability magnetic sensing at high temperatures *Mater. Res. Lett.* **8** 180–6
[30] Wang Z, Yang R and Feng P X-L 2021 Thermal hysteresis controlled reconfigurable MoS 2 nanomechanical resonators *Nanoscale* **13** 18089–95
[31] Okada Y and Tokumaru Y 1984 Precise determination of lattice parameter and thermal expansion coefficient of silicon between 300 and 1500 K *J. Appl. Phys.* **56** 314–20
[32] Liu B, Meng F, Reddy C D, Baimova J A, Srikanth N, Dmitriev S V and Zhou K 2015 Thermal transport in a graphene–MoS 2 bilayer heterostructure: a molecular dynamics study *RSC Adv.* **5** 29193–200
[33] Wu S, Wang J, Xie H and Guo Z 2020 Interfacial thermal conductance across graphene/MoS2 van der Waals heterostructures *Energies* **13** 5851
[34] Little W 1959 The transport of heat between dissimilar solids at low temperatures *Can. J. Phys.* **37** 334–49
[35] Lindsay L, Broido D and Mingo N 2010 Flexural phonons and thermal transport in graphene *Phys.l Rev. B* **82** 115427
[36] Sahoo S, Gaur A P, Ahmadi M, Guinel M J-F and Katiyar R S 2013 Temperature-dependent Raman studies and thermal conductivity of few-layer MoS2 *J. Phys. Chem. C* **117** 9042–7
[37] Wang Y, Xu N, Li D and Zhu J 2017 Thermal properties of two dimensional layered materials *Adv. Funct. Mater.* **27** 1604134
[38] Dolleman R J, Houri S, Davidovikj D, Cartamil-Bueno S J, Blanter Y M, Van Der Zant H S and Steeneken P G 2017 Optomechanics for thermal characterization of suspended graphene *Phys. Rev. B* **96** 165421
[39] Kuang Y, Lindsay L, Shi S, Wang X and Huang B 2016 Thermal conductivity of graphene mediated by strain and size *Int. J. Heat Mass Transfer* **101** 772–8
[40] Liu Y *et al* 2017 Thermal conductance of the 2D MoS2/h-BN and graphene/h-BN interfaces *Sci. Rep.* **7** 43886
[41] Ye F, Liu Q, Xu B, Feng P X-L and Zhang X 2023 Ultra-high interfacial thermal conductance via double hBN encapsulation for efficient thermal management of 2D electronics *Small* **19** 2205726